Partial oxidation of methane to synthesis gas over α-Al_2O_3-supported bimetallic Pt–Co catalysts

S. Tang, J. Lin * and K.L. Tan

Surface Science Laboratory, Department of Physics, National University of Singapore, 10 Kent Ridge Crescent, Singapore 119260
E-mail: phylinjy@nus.edu.sg

Received 14 January 1999; accepted 6 April 1999

The partial oxidation of methane to synthesis gas was studied at atmospheric pressure and in the temperature range of 550–800 °C over α-Al_2O_3-supported bimetallic Pt–Co, and monometallic Pt and Co catalysts, respectively. Both methane conversion and CO selectivity over a bimetallic $Pt_{0.5}Co_1$ catalyst were higher than those over monometallic $Pt_{0.5}$ and Co_1 catalysts. Furthermore, the addition of platinum in Pt–Co bimetallic catalysts effectively improved their resistance to carbon deposition with no coking occurring on $Pt_{0.5}Co_1$ during 80 h reaction. The FTIR study of CO adsorption observed only linearly bonded CO on bimetallic Pt–Co catalysts. TPR and XPS showed enhanced formation of a cobalt surface phase (CSP) in bimetallic Pt–Co catalysts. The origins of the good coking resistivity of bimetallic Pt–Co catalysts were discussed.

Keywords: partial oxidation of methane (POM), synthesis gas, bimetallic Pt–Co catalysts, coking, ensemble effect, cobalt surface phase (CSP)

1. Introduction

During the last few years, the partial oxidation of methane (POM) to synthesis gas has again been focused on since it produces synthesis gas with $H_2/CO \approx 2$, a composition more suitable for methanol and Fischer–Tropsch synthesis [1], and also it is an energy-efficient process [2]. Many catalysts, including supported nickel and cobalt [3–7], supported noble metals (Pd, Ir, Rh, Ru and Pt) [8–11], pyrochore containing noble metals ($Ln_2Ru_2O_7$, Ln = Lanthanide) [12,13] and perovskite oxides ($GdCoO_3$, $LaNiO_3$) [14,15], have been shown to achieve high conversion of methane and high selectivity to CO and H_2 for the POM. However, in the production of synthesis gas from methane, besides catalytic activity it is very important to investigate carbon deposition, which may lead to deactivation of catalysts and plugging of the reactor. Claridge et al. [16] have found that the relative rate of carbon deposition during the POM to synthesis gas follows the order of Ni > Pd ≫ Rh, Ru, Pt, Ir. Very little carbon deposition was observed over noble metal catalysts, especially those containing platinum and iridium.

To our knowledge, no bimetallic catalysts have been applied to the POM to synthesis gas. Bimetallic catalysts (e.g., $PtRe/Al_2O_3$, PtFe/C, $PtRu/Al_2O_3$, etc.) are attractive industrially for the addition of the second metal may modify the structure of the monometallic catalyst [17,18], increase the catalytic activity, improve the selectivity and suppress catalytic deactivation. The present study employed α-Al_2O_3-supported Pt–Co catalysts in the POM to synthesis gas and investigated the effects of the second metal on the catalytic activity and coke formation. The catalysts were characterized by TEM, TPR, *in situ* FTIR and XPS, and the mechanism of the good coking resistivity of the bimetallic Pt–Co catalysts was discussed.

* To whom correspondence should be addressed.

2. Experimental

2.1. Preparation of catalysts

The catalysts were prepared by incipient wetness impregnation of α-Al_2O_3 powder (Alfa) with a solution of the metal precursors, $PtCl_4$ (Merck) and $Co(NO_3)_2{\cdot}6H_2O$ (Merck). In order to investigate the effect of impregnation order, 0.5% Pt/1% Co/α-Al_2O_3 (wt%) catalysts were made by co-impregnation and successive impregnation including "Pt before Co" and "Co before Pt". For the co-impregnation method, the support was impregnated with a mixed aqueous solution of $PtCl_4$ and $Co(NO_3)_2{\cdot}6H_2O$. The impregnated materials were dried and calcined in air at 600 °C for 5 h. For the successive impregnation method, the support was impregnated with the aqueous solution of one component, dried and calcined in air at 600 °C for 5 h. It was then impregnated with the aqueous solution of the other component, following the same procedure as in the first step. All other Pt–Co bimetallic catalysts were prepared by the co-impregnation method. The catalysts were denoted as Pt_xCo_y, where x and y are the weight percentages of Pt and Co loading, respectively. The crystalline phases in as-prepared and reduced catalysts were characterized by XRD, as listed in table 1.

Table 1
XRD detectable crystalline phases in various Pt_xCo_y catalysts.

Catalyst	Crystalline phases	
(Pt_xCo_y)	As-prepared	Reduced
$Pt_{0.5}$	α-Al_2O_3	α-Al_2O_3
Pt_1	α-Al_2O_3	α-Al_2O_3
Pt_5	Pt, α-Al_2O_3	Pt, α-Al_2O_3
Co_1	α-Al_2O_3	α-Al_2O_3
$Co_{2.5}$	Co_3O_4, α-Al_2O_3	α-Al_2O_3
Co_5	Co_3O_4, α-Al_2O_3	Co, α-Al_2O_3
Co_{10}	Co_3O_4, α-Al_2O_3	Co, α-Al_2O_3
$Pt_{0.5}Co_1$	α-Al_2O_3	α-Al_2O_3
$Pt_{0.5}Co_{2.5}$	Co_3O_4, α-Al_2O_3	α-Al_2O_3
$Pt_{0.5}Co_5$	Co_3O_4, α-Al_2O_3	α-Al_2O_3
Pt_5Co_{10}	Co_3O_4, Pt, α-Al_2O_3	Co (very weak), α-Al_2O_3

2.2. Catalytic evaluation

The catalyts were tested at atmospheric pressure in a continuous-flow quartz microreactor (I.D. 4 mm). In every experiment 100 mg catalyst (20–35 mesh size) was reduced in a flow of hydrogen (30 ml/min) at 600 °C for 1 h. After the reduction the feed gases ($CH_4/O_2 = 2$) were introduced into the catalyst bed at a total flow rate of 93 ml/min, which corresponded to a gas hourly space velocity (GHSV) of 5.6×10^4 $cm^3\,g^{-1}\,h^{-1}$. In order to efficiently examine the resistance of the catalysts to carbon deposition, feed gases with the CH_4/O_2 ratio of 2.5 : 1 were also used since carbon deposition on the catalysts occurred easily at CH_4/O_2 ratios higher than stoichiometric ratio [19]. The reaction temperature was first maintained at 600 °C for 3 h to a steady state. Then it was changed in the range of 500–800 °C. The reaction products were measured on-line by a gas chromatograph with a molecular sieve 5A column and a Porapak Q column in series. The catalysts were evaluated in terms of methane conversion and CO selectivity, which were calculated based on the carbon numbers.

2.3. Characterization of catalysts

The amount of carbon deposited on the catalysts was measured *in situ* by mass spectrometry (Balzers QME 200), as previously described in detail [7].

Temperature-programmed reduction (TPR) was applied to monitor the reduction of the catalysts. The sample (200 mg) was outgassed at 750 °C in a flow of helium. After it cooled down to room temperature the carrier gas was changed to 10% H_2/Ar flow (40 ml/min), and the temperature was linearly increased to 800 °C at a rate of 15 °C/min. The amount of H_2 consumed was measured as a function of temperature by a thermal conductivity detector.

X-ray powder diffraction (XRD) experiments were carried out on a Philips PW 1710 X-ray diffraction spectrometer using a Cu Kα radiation source. X-ray photoelectron spectra were acquired with a VG ESCALAB MKII spectrometer, using Al Kα radiation (1486.6 eV, 120 W). An analyzer pass energy of 20 eV was adopted for all narrow scans. Pt 4d and Al 2s lines were monitored for the analysis, rather than the normally used Pt 4f and Al 2p peaks, which were hardly distinguishable due to overlapping. The C 1s peak at 285.0 eV due to adventitious carbon was used as an internal reference. Transmission electron microscopy (TEM), performed on a Jeol system with a tension voltage of 100 kV, was utilized to investigate the morphology of the coke deposited on the catalysts.

CO chemisorption and desorption were studied by *in situ* FTIR on a Perkin–Elmer 2000 equipped with a diffuse reflectance accessory and a reaction cell fitted with KBr windows. The sample was reduced in a flow of H_2 at 600 °C for 1 h, and then transferred into the sample cup in the reaction cell. It was reduced again *in situ* by hydrogen at 300 °C for 100 min, then purged by helium and cooled down to room temperature. After 30 min of CO adsorption (10% CO/He), the sample was purged by helium till the gaseous CO was removed from the cell. Spectra of the CO-adsorbed samples were then taken at various temperatures. All spectra were obtained as an average of 64 scans with a resolution of 4 cm^{-1}.

3. Results and discussion

3.1. Catalytic activity and carbon deposition

Figure 1 compares the catalytic activity of three $Pt_{0.5}Co_1$ catalysts prepared by different impregnation sequences as described in the experimental section. The catalyst prepared by co-impregnation shows the best methane conversion and CO selectivity. At temperatures below 700 °C methane conversion and CO selectivity over the catalyst prepared by successively impregnated "Pt before Co" are lower than those of co-impregnation and "Co before Pt". However, at high temperatures ($\geqslant$700 °C) their catalytic activities are close to one another. Figure 2 shows methane conversion and CO selectivity over the co-impregnated bimetallic $Pt_{0.5}Co_1$ and monometallic $Pt_{0.5}$ and Co_1 catalysts. Both methane conversion and CO selectivity over $Pt_{0.5}Co_1$ are obviously higher than those over monometallic $Pt_{0.5}$ and Co_1, while the catalytic activity of $Pt_{0.5}$ is superior to that of Co_1. Especially, at low reaction temperatures ($<$700 °C) noble metal $Pt_{0.5}$ shows much higher selectivity to CO than that of Co_1. Obviously the addition of platinum in bimetallic Pt–Co catalysts improves the CO selectivity of monometallic Co catalysts at low temperatures. The high selectivity at low reaction temperatures is very useful from a standpoint of chemical engineering. However, at higher temperatures, the CO selectivity over the Co_1 catalyst increases rapidly, getting close to that of $Pt_{0.5}$ at 800 °C. This trend is also observable in figure 1, for the bimetallic $Pt_{0.5}Co_1$ catalyst prepared by the successive impregnation of "Pt before Co", in which more cobalt component may exist on the catalyst surface, so that its catalytic activity is similar to that of the monometallic Co_1 catalyst.

The resistance of the catalysts to carbon deposition was investigated under thermodynamically severe conditions (GHSV $= 5.4 \times 10^4$ $cm^3\,g^{-1}\,h^{-1}$, 750 °C and a high

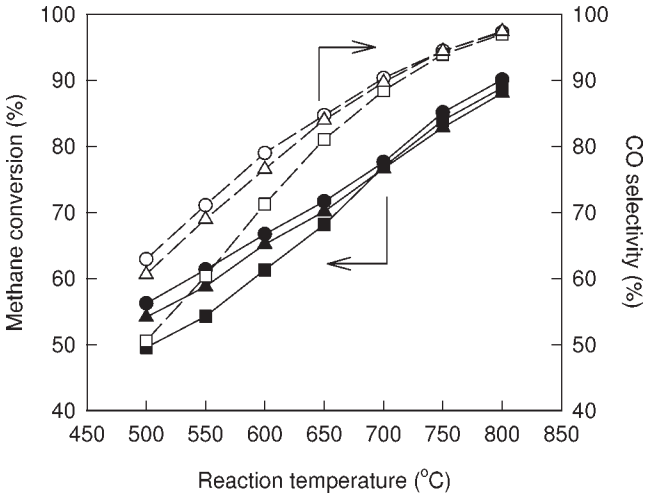

Figure 1. CH_4 conversion (solid symbols) and CO selectivity (open symbols) as a function of reaction temperature over three $Pt_{0.5}Co_1$ catalysts prepared by different impregnation orders ($CH_4/O_2 = 2$, GHSV $= 5.6 \times 10^4$ cm^3 g^{-1} h^{-1}): (○) co-impregnation, (△) "Co before Pt" and (□) "Pt before Co".

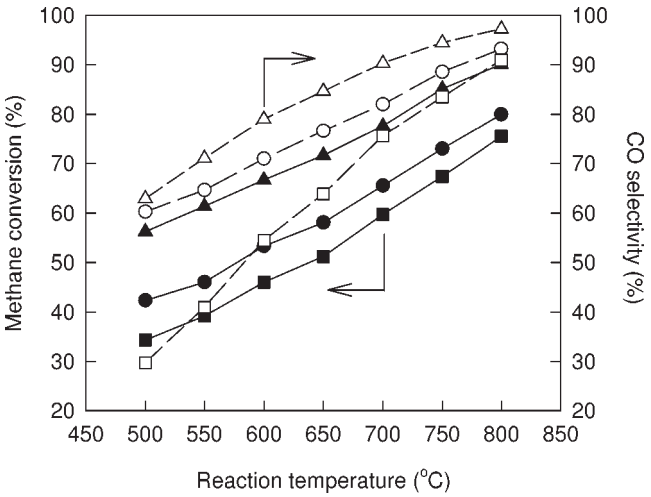

Figure 2. The effect of reaction temperature on CH_4 conversion (solid symbols) and CO selectivity (hollow symbols) over co-impregnated bimetallic $Pt_{0.5}Co_1$ and monometallic $Pt_{0.5}$ and Co_1 catalysts ($CH_4/O_2 = 2$, GHSV $= 5.6 \times 10^4$ cm^3 g^{-1} h^{-1}): (△) $Pt_{0.5}Co_1$, (○) $Pt_{0.5}$ and (□) Co_1.

ratio of $CH_4/O_2 = 2.5$). The average rates of carbon deposition on various samples are given in table 2. Supported monometallic Pt catalysts show an excellent resistance to carbon deposition since no coke was observed over the $Pt_{0.5}$ and Pt_1 catalysts after reaction of 5 h. For supported monometallic cobalt catalysts, the average rates of carbon deposition appreciably increase with the increase of cobalt loading, with 0.40 g(carbon) g^{-1}(cat.) h^{-1} for Co_1 while 10.08 g(carbon) g^{-1}(cat.) h^{-1} for Co_5. For the bimetallic Pt–Co catalysts the coking rate is reduced by a half, with 0.20 and 4.56 g(carbon) g^{-1}(cat.) h^{-1} for $Pt_{0.5}Co_1$ and $Pt_{0.5}Co_5$, respectively. Actually under approximate GHSV (5.6×10^4 cm^3 g^{-1} h^{-1}) and 750 °C, but with feed gases of stoichiometric ratio ($CH_4/O_2 = 2$) no coking was measured on the $Pt_{0.5}Co_1$ catalyst after 80 h of reaction, while both the

Table 2
The effect of catalyst composition on the average rates of coking (750 °C, $CH_4/O_2 = 2.5$, GHSV $= 5.4 \times 10^4$ cm^3 g^{-1} h^{-1}).

Catalyst (Pt_xCo_y)	Average rate of coke $\times 10^2$ g(carbon) g^{-1}(cat.) h^{-1}
$Pt_{0.5}$	–[a]
Pt_1	–[a]
Co_1	0.40[a]
$Co_{2.5}$	1.37[a]
Co_5	10.08[b]
$Pt_{0.5}Co_1$	0.20[a]
$Pt_{0.5}Co_{2.5}$	0.62[a]
$Pt_{0.5}Co_5$	4.56[b]

[a] Total reaction time: 5 h.
[b] Total reaction time: 1 h.

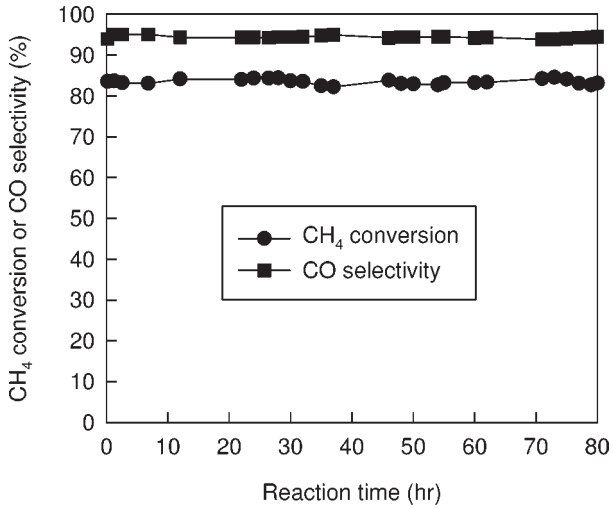

Figure 3. Catalytic activity and stability over bimetallic $Pt_{0.5}Co_1$ catalyst ($T = 750$ °C, $CH_4/O_2 = 2$, GHSV $= 5.6 \times 10^4$ cm^3 g^{-1} h^{-1}).

activity and selectivity remain stable, as shown in figure 3. This indicates that the addition of platinum to monometallic cobalt catalysts effectively inhibits carbon deposition.

The micrography of the coke on the catalysts was taken by TEM. As presented in figure 4, the coke on both monometallic $Co_{2.5}$ (figure 4(a)) and bimetallic $Pt_{0.5}Co_1$ (figure 4(b)) exists mainly in the form of carbon whisker. It is generally suggested that whisker carbon does not alter the rate of synthesis gas production [19]. This may explain why no deactivation was observed over the monometallic Co_5 catalyst even though almost 10 wt% coke was deposited on it. Nevertheless, coking is still harmful to catalytic reaction since a large amount of whisker carbon would lead to shattering of the catalysts and plugging of the reactor as observed over Co_5 catalyst.

3.2. Temperature-programmed reduction (TPR)

The reduction behavior of the catalysts was investigated by TPR. As shown in figure 5, the TPR peak for the $Pt_{0.5}$ catalyst is rather weak (figure 5(a)). One strong peak centered at 370 °C with a relatively weak peak at 325 °C

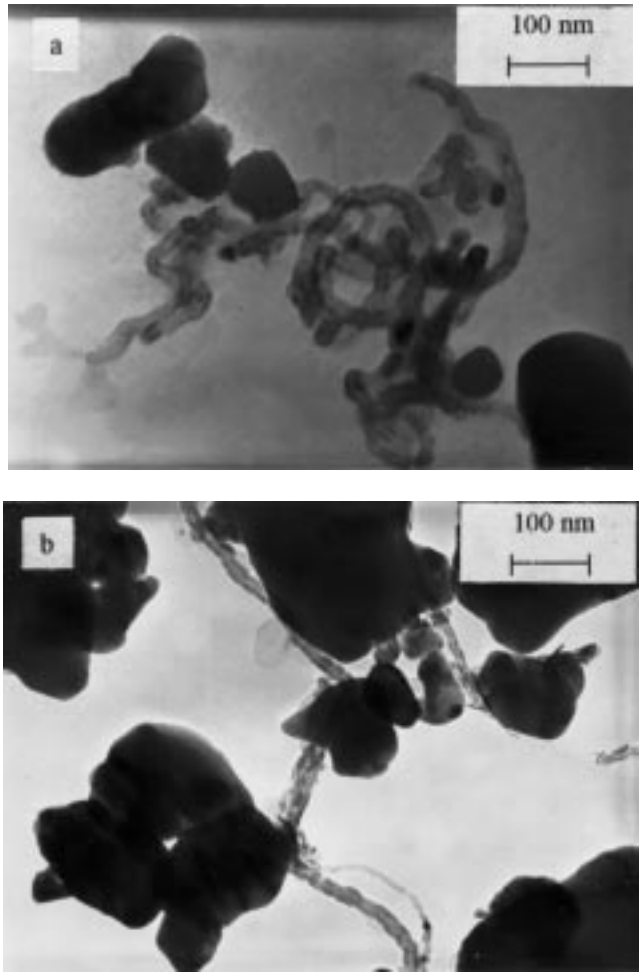

Figure 4. TEM micrographs of coke deposited on catalysts after the reaction with $CH_4/O_2 = 2.5$: (a) $Co_{2.5}$ and (b) $Pt_{0.5}Co_1$.

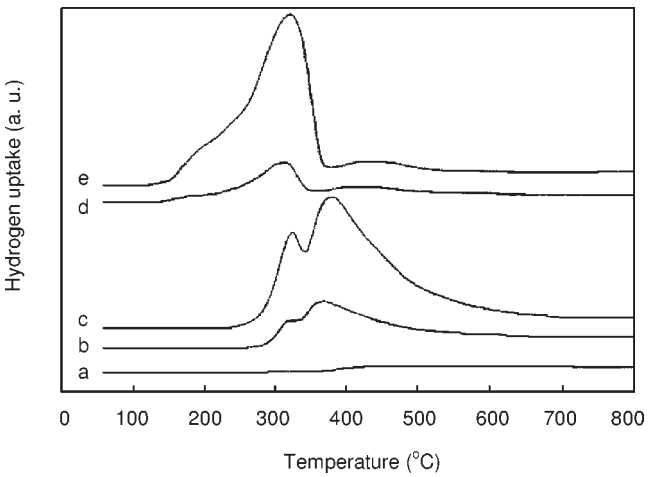

Figure 5. The TPR profiles of the catalysts, which were taken under identical conditions: (a) $Pt_{0.5}$, (b) Co_1, (c) $Co_{2.5}$, (d) $Pt_{0.5}Co_1$ and (e) $Pt_{0.5}Co_{2.5}$.

is observed for the Co_1 catalyst (figure 5(b)) while one strong peak at 310 °C with a shoulder at lower temperature side for the bimetallic $Pt_{0.5}Co_1$ catalyst (figure 5(d)). The TPR profile of the $Co_{2.5}$ is similar to that of Co_1, and the TPR profile of $Pt_{0.5}Co_{2.5}$ similar to that of $Pt_{0.5}Co_1$. Obviously, bimetallic catalysts have lower reduction temperatures. Since the monometallic $Pt_{0.5}$ catalyst shows only a very weak TPR signal, the TPR peaks of the bimetallic Pt–Co catalyst should mainly derive from the reduction of cobalt oxides. This is in agreement with the obtained XRD results that metallic Pt is detected in the bulk of as-prepared catalysts while cobalt exists as Co_3O_4 (table 1). The addition of platinum lowers the reduction temperature of cobalt oxides in bimetallic Pt–Co/α-Al_2O_3 catalysts. However, it should be mentioned that the total area of TPR peaks of the bimetallic Pt–Co sample is less than that of the corresponding monometallic Co sample, i.e., 1.0 for Co_1 vs. 0.70 for $Pt_{0.5}Co_1$, and 3.3 for $Co_{2.5}$ vs. 2.87 for $Pt_{0.5}Co_{2.5}$, as shown in table 3. This implies that the addition of platinum actually increases the amount of unreducible components. As suggested later in the XPS analysis section, the unreducible component is most probably cobalt surface phase (CSP).

Table 3
The relative total area of TPR peaks on various Pt_xCo_y catalysts.

Catalyst	Relative area of TPR[a]
$Pt_{0.5}$	Trivial
Co_1	1.00
$Pt_{0.5}Co_1$	0.70
$Co_{2.5}$	3.30
$Pt_{0.5}Co_{2.5}$	2.87

[a] The total area of Co_1 is taken as 1.00.

3.3. CO adsorption and desorption

The CO adsorption and desorption were studied by FTIR. At room temperature we have not found detectable adsorption of CO over the reduced $Pt_{0.5}$, Co_1 and $Pt_{0.5}Co_1$ catalysts, probably due to low metal loading. In order to reveal clearly the interaction between metal Pt and Co, we performed CO adsorption study on the Pt_5, Co_{10} and Pt_5Co_{10} catalysts with high metal loading, ten times of those for $Pt_{0.5}$, Co_1 and $Pt_{0.5}Co_1$, respectively. On reduced Co_{10} no molecular CO adsorption was detected, but the dissociative adsorption of CO was evidenced by the observation of vibrations of Co–C near 900 cm^{-1} and Co–O near 540 cm^{-1} at about 200 °C [20]. On Pt_5 one strong CO band near 2075 cm^{-1} and one weak band near 1838 cm^{-1} were observed at room temperature (see figure 6). The IR band at 2075 cm^{-1} is attributed to terminally-bonded CO and the band at 1838 cm^{-1} to bridged or triply-bonded CO on Pt metal [21]. Increasing the temperature up to 120 °C affects the spectrum little. However, at 143 °C the bridged adsorption peak disappeared while the linear CO species were observed with a very low intensity. At 154 °C the linear adsorption species were also eliminated. On the reduced Pt_5Co_{10} bimetallic catalyst there was only one weak linear CO adsorption peak near 2075 cm^{-1} at room temperature (figure 7). It vanished completely at about 198 °C. The lack of the bridged CO may imply that metal Pt atoms

are surrounded or diluted by metal Co atoms in the reduced Pt_5Co_{10} catalyst. A similar effect was previously reported by Mériaudeau et al. [22], who investigated the CO adsorption over Pt_xIn_y bimetallics in NaY zeolite, and by Guczi et al. [17,18], who studied the Pt–Co hydrogenation catalysts by *in situ* XPS. This is further supported by EXAFS analysis of Pt–Co/Al_2O_3, in which traces of bimetallic particles were detected and considered to result from the intimate contact between Pt and Co [23]. It is suggested that CO dissociation on transition metal surfaces is initiated via adsorption at multiply coordinated sites [24,25]. The ensemble effect in Pt–Co bimetallic catalysts appears to reduce the multiply coordinated cobalt sites and thus the dissociative adsorption of CO. Therefore, carbon deposition will be effectively inhibited. Besides, Rostrup-Nielsen [26] found that catalysts with larger metal clusters were more susceptible to coke generation. The addition of platinum may limit the sintering of metallic Co and the formation of large Co clusters so that our XRD results show no metallic Co phase in the bimetallic $Pt_{0.5}Co_5$ catalyst, but metallic Co phase in monometallic Co_5. This may explain the long-hour stability of catalytic activity over $Pt_{0.5}Co_1$ catalyst.

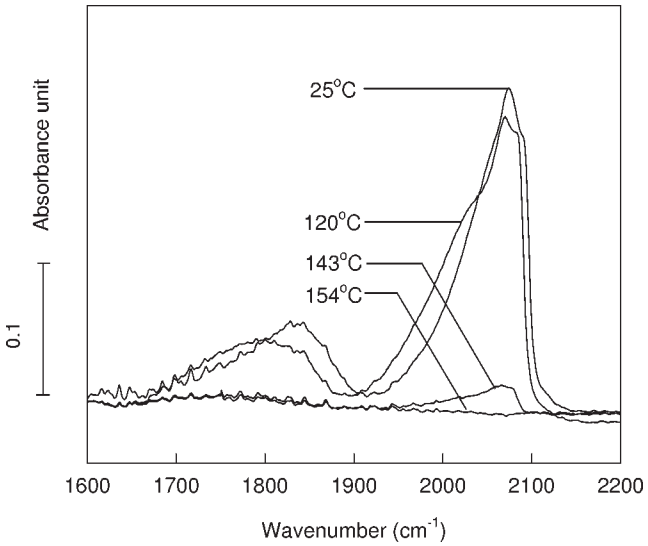

Figure 6. FTIR spectra of adsorbed CO on reduced Pt_5 at various temperatures.

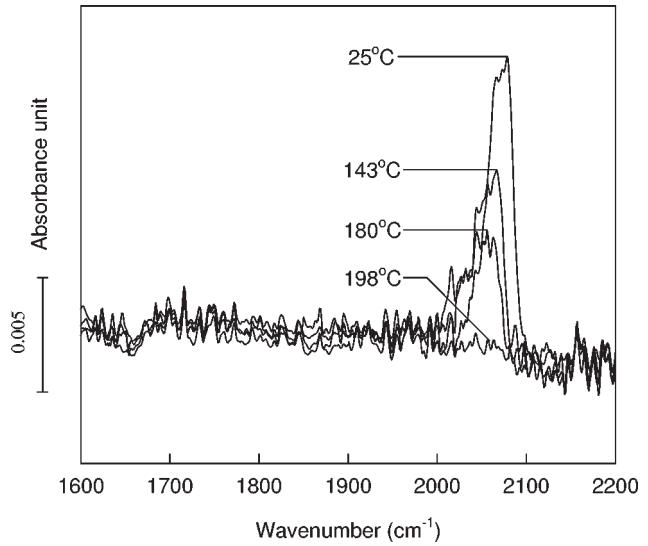

Figure 7. FTIR spectra of adsorbed CO on reduced Pt_5Co_{10} at various temperatures.

3.4. X-ray photoelectron spectroscopy (XPS)

The binding energy (BE) values of Pt $4d_{5/2}$ and Co $2p_{3/2}$ are given in table 4 and the fitted XPS spectra of Co 2p are shown in figures 8 and 9 for the as-prepared and reduced catalysts, respectively. The Co $2p_{3/2}$ peak of monometallic Co_{10} in the as-prepared state is located at 780.2 eV with no shake-up satellite (see figure 8(a)) while the bimetallic Pt_5Co_{10} sample has its Co $2p_{3/2}$ centered at 780.5 eV with a shake-up satellite near 786.0 eV (figure 8(b)). According to the BE values of Co $2p_{3/2}$, the intensity ratio of the shake-up satellite and spin–orbit coupling values [27–29], the cobalt in the as-prepared Co_{10} is assigned to Co_3O_4 (Co $2p_{3/2}$ = 780.0–780.6 eV, weak satellite and 15 eV of spin–orbit splitting) while there exists a large amount of Co^{2+} (Co $2p_{3/2}$ = 780.0–780.6 eV, strong satellite and 16 eV of spin–orbit splitting) besides Co^{3+} in the as-prepared Pt_5Co_{10}. After reduction Co^{2+} becomes predominant in monometallic Co_{10}, as shown by the presence of a strong shake-up satellite (figure 9(a)). A new peak of lower BE (Co $2p_{3/2}$ = 778 eV) indicates that certain amount of Co has been reduced to metal. The same is true for the reduced Pt_5Co_{10} catalyst. However, the main component peak in reduced Pt_5Co_{10} catalysts is at 781.2 eV, beyond the BE range normally assigned for Co_3O_4/CoO (780.0–780.6 eV). As cobalt surface phase (CSP) is known

Table 4
Binding energy of Pt $4d_{5/2}$ and Co $2p_{3/2}$.

Catalyst	Pt $4d_{5/2}$ (eV)		Co $2p_{3/2}$ (eV)	
	As-prepared	Reduced	As-prepared	Reduced
Pt_5	315.7 (Pt^{2+}) 318.2 (Pt^{4+})	314.8 (Pt^0) 318.0 (Pt^{4+})	–	–
Co_{10}	–	–	780.2 (Co^{3+})	778 (Co^0) 780.6 (Co^{2+}/Co^{3+})
Pt_5Co_{10}	318.0 (Pt^{4+})	314.9 (Pt^0)	– 780.5 (Co^{2+}/Co^{3+})	778 (Co^0) 781.2 (CSP/Co^{2+})

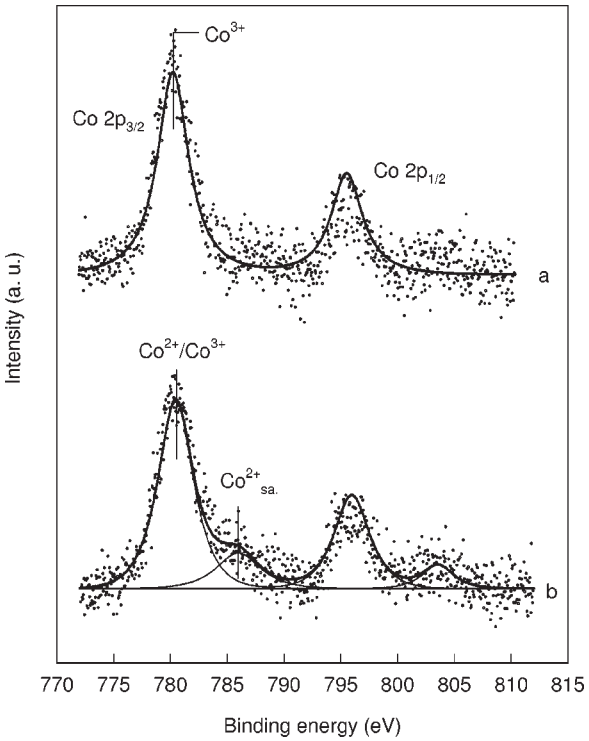

Figure 8. Co 2p XPS spectra of the catalysts in the as-prepared states: (a) Co_{10} and (b) Pt_5Co_{10}.

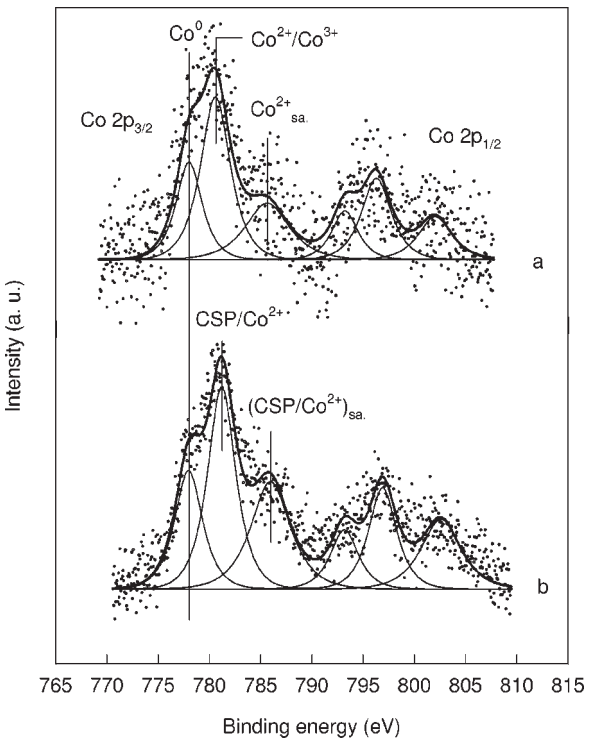

Figure 9. Co 2p XPS spectra of the catalysts after reduction at 600 °C: (a) Co_{10} and (b) Pt_5Co_{10}.

to have Co $2p_{3/2}$ in the range of 781.5–781.7 eV with a strong shake-up satellite [18], spectrum 9(b) may illustrate that the addition of platinum has promoted the formation of CSP. This is also supported by former TPR results since it is difficult to reduce CSP. It is worthwhile to mention that similar XPS spectra of Pt $4d_{5/2}$ and Co $2p_{3/2}$ were obtained from as-prepared and reduced $Pt_{0.5}$, Co_1 and $Pt_{0.5}Co_1$ catalysts, although the signals of these spectra were weak. It is assumed that CSP is highly dispersed in monolayer thickness, and strongly interacts with support or/and lattice oxygen [30]. This strong interaction between metal and support will inhibit the Co surface reconstruction via bond relaxation, hence carbon diffusion into cobalt lattice, which may lead to the formation of carbon whiskers, may be prevented to some extent [7,31,32].

4. Conclusion

In summary, bimetallic Pt–Co catalysts have shown better CH_4 conversion and CO selectivity than monometallic Pt and Co catalysts. In particular, the $Pt_{0.5}Co_1$ catalyst has high and rather stable catalytic activity during 80 h of POM reaction, with no coke deposited on it under stoichiometric feeding condition ($CH_4/O_2 = 2$). These findings may imply that it is possible to partially replace noble Pt by Co, to largely lower the cost of monometallic Pt catalysts without sacrificing the catalytic activity, selectivity and stability, in the POM to synthesis gas.

The addition of platinum can obviously improve the coking resistivity of monometallic Co catalysts, probably due to the following factors: (1) ensemble effect decreasing the number of multiply coordinated cobalt sites, on which CO is dissociated; (2) strong metal–support interaction resulting in the formation of CSP, which prevents the carbon diffusion into cobalt lattice.

References

[1] R.S. Drago, K. Jurczyk, N. Kob, A. Bhattacharyya and J. Masin, Catal. Lett. 51 (1998) 177.
[2] N. Nichio, M. Lasella, O. Ferretti, M.Gonzãlez, C. Nicot, B. Moraweck and R. Frety, Catal. Lett. 42 (1996) 65.
[3] D. Dissanayake, M.P. Rosynek, K.C.C. Kharas and J.H. Lunsford, J. Catal. 132 (1992) 117.
[4] V.R. Choudhary, A.M. Rajput and V.H. Rane, J. Phys. Chem. 96 (1992) 8686.
[5] Y.F. Chang and H. Heineman, Catal. Lett. 21 (1993) 215.
[6] T. Hayakawa, H. Harihara, A.G. Andersen, A.P.E. York, K. Suzuki, H. Yasuda and K. Takehira, Angew. Chem. Int. Ed. Engl. 35 (1996) 192.
[7] S. Tang, J. Lin and K.L. Tan, Catal. Lett. 51 (1998) 169.
[8] L.D. Schmidt and D.A. Hickman, Science 259 (1993) 343; J. Catal. 138 (1992) 267.
[9] P.M. Tornianan, X. Chu and L.D. Schmidt, J. Catal. 146 (1994) 1.
[10] P.D.F. Vernon, M.L.H. Green, A.K. Cheetham and A.T. Ashcroft, Catal. Lett. 6 (1990) 181.
[11] A.K. Bhattacharaya, J.A. Breach, S. Chand, D.K. Ghorai, A. Hartridge, J. Keary and K.K. Mallick, Appl. Catal. A 80 (1992) L1.
[12] A.T. Ashcroft, A.K. Cheetham, J.S. Food, M.L.H. Green, C.P. Gray, A.G. Murrell and P.D.F. Vernon, Nature 344 (1990) 319.
[13] R.H. Jones, A.T. Ashcroft, D. Waller, A.K. Cheetham and J.M. Thomas, Catal. Lett. 8 (1991) 169.

[14] R. Lago, G. Bini, M.A. Peña and J.L.G. Fierro, J. Catal. 167 (1997) 198.
[15] V.R. Choudhary, B.S. Uphade and A.A. Belhekar, J. Catal. 163 (1996) 312.
[16] J.B. Claridge, M.L.H. Green, S.C. Tsang, A.P.E. York, A.T. Ashcroft and P.D. Battle, Catal. Lett. 22 (1993) 299.
[17] L. Guczi, G. Lu and Z. Zsoldos, Catal. Today 17 (1993) 459.
[18] Z. Zsoldos and L. Guczi, J. Phys. Chem. 96 (1992) 9393.
[19] S.C. Tsang, J.B. Claridge and M.L.H. Green, Catal. Today 23 (1995) 3.
[20] R.A. Nyquist and R.O. Kagel, in: *The Handbook of Infrared and Raman Spectra of Inorganic Compounds*, Vol. 4 (Academic Press, New York, 1997) p. 218.
[21] F.J.C. Toolenaar, F. Stoop and V.J. Ponec, J. Catal. 82 (1983) 1.
[22] P. Mériaudeau, A. Thangaraj, J.F. Dutel, P. Gelin and C. Naccache, J. Catal. 163 (1996) 338.
[23] S. Zyade, F. Garin and G. Maire, New J. Chem. 11 (1987) 429.
[24] F. Zaera, E. Kollin and J.L. Gland, Chem. Phys. Lett. 121 (1985) 464.
[25] G. Blyholder and M. Lawless, Surf. Sci. 290 (1993) 155.
[26] J.R. Rostrup-Nielsen, J. Catal. 85 (1984) 31.
[27] T.J. Chuang, C.R. Brundle and D.W. Rice, Surf. Sci. 59 (1976) 413.
[28] D. Briggs and V.A. Gibson, Chem. Phys. Lett. 25 (1974) 493.
[29] K. Sato, Y. Inoue, I. Kojima, E. Miyazaki and I. Yasumori, J. Chem. Soc. Faraday Trans. I 80 (1984) 841.
[30] M.A. Stranick, M. Hualla and D.M. Hercules, J. Catal. 103 (1987) 151.
[31] M.C.J. Bradford and M.A. Vannice, Appl. Catal. A 142 (1996) 73.
[32] R. Blom, I.M. Dahl, Å. Slagtern, B. Sortland, A. Spjelkavik and E. Tangstad, Catal. Today 21 (1994) 535.